



## Research Paper

# Achieving efficient room-temperature catalytic H<sub>2</sub> evolution from formic acid through atomically controlling the chemical environment of bimetallic nanoparticles immobilized by isoreticular amine-functionalized metal-organic frameworks

Jia Cheng, Xiaojun Gu\*, Penglong Liu, Hao Zhang, Lunliang Ma, Haiquan Su\*

Inner Mongolia Key Laboratory of Coal Chemistry, School of Chemistry and Chemical Engineering, Inner Mongolia University, Hohhot 010021, Inner Mongolia, China



## ARTICLE INFO

## Article history:

Received 19 March 2017

Received in revised form 2 June 2017

Accepted 27 June 2017

Available online 28 June 2017

## Keywords:

H<sub>2</sub> evolution

Controlled chemical environment

Room-temperature catalysis

Hydrogen storage materials

Metal-organic frameworks

## ABSTRACT

From the viewpoint of controlling the catalytic performance of supported metal nanoparticles (NPs) through tuning their chemical environment in the atom level, we have used electron-donating amino groups and three organic amine molecules to modify the organic linkers and unsaturated coordination  $\text{Cr}^{3+}$  sites in one porous metal-organic framework MIL-101 with atomically precise structures, respectively, and then we have prepared a series of AuPd NPs immobilized by the two types of functional MIL-101 supports. The as-synthesized AuPd NPs were used for the catalytic dehydrogenation of formic acid ( $\text{HCOOH}$ ) and the results showed that these catalysts exhibited remarkably different activities and H<sub>2</sub> selectivities at 298 K. Particularly, the AuPd NPs immobilized by MIL-101-NH<sub>2</sub> presented 100% of H<sub>2</sub> selectivity and the highest activity because of the synergistic steric and electronic effects, which were related to the activation of  $\text{HCOOH}$  and enrichment of electron density of active Pd species. The investigation of UV-vis spectroscopy showed that the reaction between the mixed metal ions ( $\text{AuCl}_4^-$  and  $\text{PdCl}_4^{2-}$ ) and the four functional MIL-101 supports generated four different coordination complex intermediates, which played an important role in yielding AuPd NPs with different chemical environment and inducing different catalytic performance.

© 2017 Elsevier B.V. All rights reserved.

## 1. Introduction

The catalytic activity and selectivity of heterogeneous catalysts are highly determined by the chemical environment around active species [1–7]. Consequently, various methods have been explored to tune the environment, among which the inorganic supports such as  $\text{Al}_2\text{O}_3$ ,  $\text{SiO}_2$  and zeolites with high surface areas have been usually selected to guide the formation of active metal or metal oxide nanoparticles (NPs) [8–12]. The catalyst environment in these systems is heterogeneous in the spatial arrangement of the chemical functionalities. Therefore, it is necessary to design nanocatalysts with the chemical environment processing atomic precision to achieve the molecular control during catalytic reactions, which can simulate the enzymatic and homogeneous catalysis [13–15]. However, in heterogeneous catalysts, it is quite difficult to achieve this

object, mainly owing to the lack of catalyst supports with atomic-level tunability. Among the catalyst supports, porous metal-organic framework (MOFs) constructed by metal ions/clusters and organic ligands show perfect performance, because they not only exhibit high surface area but also have precisely controllable crystal structures and easy organic functionalization through the post-synthetic modification or ligand design in the atom level [16–24]. In the past decade, the introduction of functional groups into MOFs has caused the different chemical environment around the encapsulated guest molecules. With these merits, they have been broadly used in various applications, such as the gas sorption and uptake selectivity as well as the water stability [25–30]. However, there are rarely systematical studies on how to use the functional groups in MOFs to tune the well-defined chemical environment around the catalytic active species, such as encapsulated or supported metal NPs, thus to achieve the control of their catalytic properties, including activity and selectivity of target products [31,32].

Hydrogen (H<sub>2</sub>) is considered as a promising clean energy carrier for future application because of its high energy density and

\* Corresponding authors.

E-mail addresses: [xiaojun.gu@yahoo.com](mailto:xiaojun.gu@yahoo.com) (X. Gu), [haiquansu@yahoo.com](mailto:haiquansu@yahoo.com), [haiquansu@sina.com](mailto:haiquansu@sina.com) (H. Su).

renewability, but the safe, efficient storage and release of H<sub>2</sub> are still the subject of intensive research [33–40]. Formic acid (HCOOH, FA), a major product of biomass processing with high energy density, has received considerable attention for H<sub>2</sub> storage and generation. The hydrogen stored in FA can be released via the catalytic dehydrogenation pathway (HCOOH → H<sub>2</sub> + CO<sub>2</sub>) [41–52]. The recent studies show that palladium (Pd) is the active species for the catalytic dehydrogenation of FA and the size of Pd-based NPs plays an important role in the catalytic process [53–63]. Besides, optimizing the functional groups in the supports also affect the interaction between FA molecules and the functional groups in the supports. It could be favorable to tune the chemical environment around the NPs to achieve the regulation of the activation ways of FA molecules and the electron density of Pd species as well as the resulting catalytic dehydrogenation of FA at mild conditions, especially at room temperature (298 K).

Herein, on the basis of that (i) MOFs functionalized by organic groups or organic molecules have the atomically precise structures and (ii) the steric and electronic effects of the organic ligands play a synergistic role in the activity and selectivity in an enzymatic or homogeneous catalyst [64–69], we have used NH<sub>2</sub> groups or different organic amines to modify the organic linkers and unsaturated coordination Cr<sup>3+</sup> sites in one of porous MOFs, MIL-101, respectively [70–72]. Then we have developed a series of AuPd NPs immobilized by the isoreticular functional MIL-101 frameworks, which were used as catalysts for FA dehydrogenation. Interestingly, through tuning the functionalization of MIL-101 in different sites, the resultant catalysts exhibited remarkably different activities and H<sub>2</sub> selectivities at 298 K. Moreover, the possible catalytic mechanism was also discussed.

## 2. Experimental

### 2.1. Chemicals

All chemicals were commercial and used without further purification. Formic acid (HCOOH, Sigma-Aldrich, 99%), sodium formate (HCOONa, SF, Sigma-Aldrich, ≥99.0%), tetrachloroauric acid (HAuCl<sub>4</sub>·4H<sub>2</sub>O, Sinopharm Chemical Reagent Co., Ltd., Au >47.8%), palladium chloride (PdCl<sub>2</sub>, Sinopharm Chemical Reagent Co., Ltd., Pd >59.0%), sodium borohydride (NaBH<sub>4</sub>, J&K Scientific Ltd., 98.0%), 3,3'-diaminodipropylamine (C<sub>6</sub>H<sub>17</sub>N<sub>3</sub>, DADPA, Sigma-Aldrich, 98%), diethylenetriamine (C<sub>4</sub>H<sub>13</sub>N<sub>3</sub>, DETA, J&K Scientific Ltd., 99.0%), ethylenediamine (C<sub>2</sub>H<sub>8</sub>N<sub>2</sub>, EDA, Sinopharm Chemical Reagent Co., Ltd., ≥99.0%), sodium hydroxide (NaOH, Sinopharm Chemical Reagent Co., Ltd., >99.0%), sodium chloride (NaCl, Sinopharm Chemical Reagent Co., Ltd., ≥99.8%), hydrofluoric acid (HF, Sinopharm Chemical Reagent Co., Ltd., ≥40.0%) hydrochloric acid (HCl, Beijing Chemical Plant, AR), nitric acid (HNO<sub>3</sub>, Beijing Chemical Plant, AR), sulfuric acid (H<sub>2</sub>SO<sub>4</sub>, Tianjin Chemical Reagent Factory, 95–98%), tin chloride dihydrate (SnCl<sub>2</sub>·2H<sub>2</sub>O, Sinopharm Chemical Reagent Co., Ltd., AR), zinc nitrate hexahydrate (Zn(NO<sub>3</sub>)<sub>2</sub>·6H<sub>2</sub>O, Sinopharm Chemical Reagent Co., Ltd., ≥99.0%), chromium nitrate nonahydrate (Cr(NO<sub>3</sub>)<sub>3</sub>·9H<sub>2</sub>O, Sinopharm Chemical Reagent Co., Ltd., ≥99.0%), 2-aminoterephthalic acid (C<sub>8</sub>H<sub>7</sub>NO<sub>4</sub>, Sigma-Aldrich, 99.0%), terephthalic acid (C<sub>8</sub>H<sub>6</sub>O<sub>4</sub>, Aladdin, 99%), N,N-diethylformamide (DEF, Tianjin Fengchuan Chemical Reagent Technologies Co., Ltd., ≥99.5%), chloroform (CHCl<sub>3</sub>, Aladdin, ≥99.5%), dichloromethane (CH<sub>2</sub>Cl<sub>2</sub>, Tianjin Fengchuan Chemical Reagent Technologies Co., Ltd., ≥99.5%), tetraethyl orthosilicate (TEOS, Sinopharm Chemical Reagent Co., Ltd., ≥99%), poly(ethylene glycol)-blockpoly(propylene glycol)-block-poly(ethylene glycol) (P<sub>123</sub>, Sigma-Aldrich), (3-aminopropyl)-triethoxysilane (APTES, Sigma-Aldrich, 99%) and ethanol (C<sub>2</sub>H<sub>5</sub>OH, Tianjin Fengchuan

Chemical Reagent Technologies Co., Ltd., >99.7%) were obtained. Deionized water was used in all the experiments.

### 2.2. Synthesis and catalytic study

#### 2.2.1. Synthesis of functional MIL-101 frameworks

For the synthesis of the first type of functional MIL-101 species, the functionalization of organic linkers in MIL-101 using NH<sub>2</sub> groups was carried out and the product was noted as MIL-101-NH<sub>2</sub>. Firstly, the nitration of MIL-101 (0.1 g) was performed using 12 mL of acid (HNO<sub>3</sub> conc. and H<sub>2</sub>SO<sub>4</sub> conc.) for 5 h under ice cooling, leading to NO<sub>2</sub>-functionalized MIL-101, which was noted as MIL-101-NO<sub>2</sub>. Secondly, the reduction of NO<sub>2</sub> groups in MIL-101-NO<sub>2</sub> to NH<sub>2</sub> groups was performed using SnCl<sub>2</sub>·2H<sub>2</sub>O as reductant to form MIL-101-NH<sub>2</sub>. For the synthesis of the second type of MIL-101 species functionalized by DADPA containing NH<sub>2</sub> groups, which was noted as DADPA-MIL-101, MIL-101 (0.1 g) was immersed and stirred in 10 mL CH<sub>2</sub>Cl<sub>2</sub> solution of DADPA (0.15 mL) at 298 K for 24 h, leading to the formation of DADPA-MIL-101. The isoreticular MIL-101 species functionalized by DETA and EDA containing NH<sub>2</sub> groups, which were noted as DETA-MIL-101 and EDA-MIL-101, respectively, were also synthesized using the similar process to that of DADPA-MIL-101 except the utilization of DETA and EDA as functional molecules.

#### 2.2.2. Synthesis of catalysts

The aqueous solution of Na<sub>2</sub>PdCl<sub>4</sub> was prepared by dissolving PdCl<sub>2</sub> (1.0 g) and NaCl (0.65 g) into 50 mL of water with magnetic stirring for 10 h. All the catalysts were synthesized using an impregnation-reduction process. Typically, for the synthesis of Au<sub>1</sub>Pd<sub>1.5</sub>/MIL-101-NH<sub>2</sub>, HAuCl<sub>4</sub>·4H<sub>2</sub>O (0.0165 g, 0.04 mmol) and Na<sub>2</sub>PdCl<sub>4</sub> (0.0177 g, 0.06 mmol) were dispersed in deionized H<sub>2</sub>O (4 mL). Then, activated MIL-101-NH<sub>2</sub> (0.04 g), which was dried at 150 °C under vacuum for 12 h, was added into the solution with stirring for 2 h. After that, the deionized H<sub>2</sub>O (2 mL) containing NaBH<sub>4</sub> (0.06 g) was added into the above mixture, which was vigorously stirred for 2 h to obtain a black suspension, Au<sub>1</sub>Pd<sub>1.5</sub>/MIL-101-NH<sub>2</sub>, for the catalytic reaction.

In order to study the effects of different functional supports and the molar ratios of Au/Pd on the catalytic hydrogen evolution, other nineteen bimetallic and monometallic catalysts, namely, Au<sub>1</sub>Pd<sub>1.5</sub>/DADPA-MIL-101, Au<sub>1</sub>Pd<sub>1.5</sub>/DETA-MIL-101, Au<sub>1</sub>Pd<sub>1.5</sub>/EDA-MIL-101, Au<sub>1</sub>Pd<sub>1.5</sub>/MIL-101-NO<sub>2</sub>, Au<sub>1</sub>Pd<sub>1.5</sub>/MIL-101, Au<sub>1</sub>Pd<sub>1.5</sub>/MOF-5-NH<sub>2</sub>, Au<sub>1</sub>Pd<sub>1.5</sub>/MOF-5, Au<sub>1</sub>Pd<sub>1.5</sub>/SBA-15-NH<sub>2</sub>, Au<sub>1</sub>Pd<sub>1.5</sub>/SBA-15, Au<sub>1</sub>Pd<sub>2</sub>/MIL-101-NH<sub>2</sub>, Au<sub>1</sub>Pd<sub>1</sub>/MIL-101-NH<sub>2</sub>, Au<sub>1.5</sub>Pd<sub>1</sub>/MIL-101-NH<sub>2</sub>, Au<sub>2</sub>Pd<sub>1</sub>/MIL-101-NH<sub>2</sub>, Au/MIL-101-NH<sub>2</sub>, Pd/MIL-101-NH<sub>2</sub>, Pd/DADPA-MIL-101, Pd/DETA-MIL-101, Pd/EDA-MIL-101 and Pd/MIL-101 were synthesized using the similar process to that of Au<sub>1</sub>Pd<sub>1.5</sub>/MIL-101-NH<sub>2</sub> (see the Supporting Information).

#### 2.2.3. Catalytic study on H<sub>2</sub> evolution from HCOOH

For the catalytic study, the as-synthesized catalyst was kept in a two-necked flask. One neck was connected to a gas burette and the other was connected to a pressure-equalization funnel to introduce FA-SF aqueous solution. The catalytic reaction began once the FA-SF solution was injected into the flask. The evolution of gas was monitored using the gas burette. The catalytic reaction was carried out at different temperatures under ambient atmosphere. The atmospheric pressure in Hohhot was 88.8 kPa.

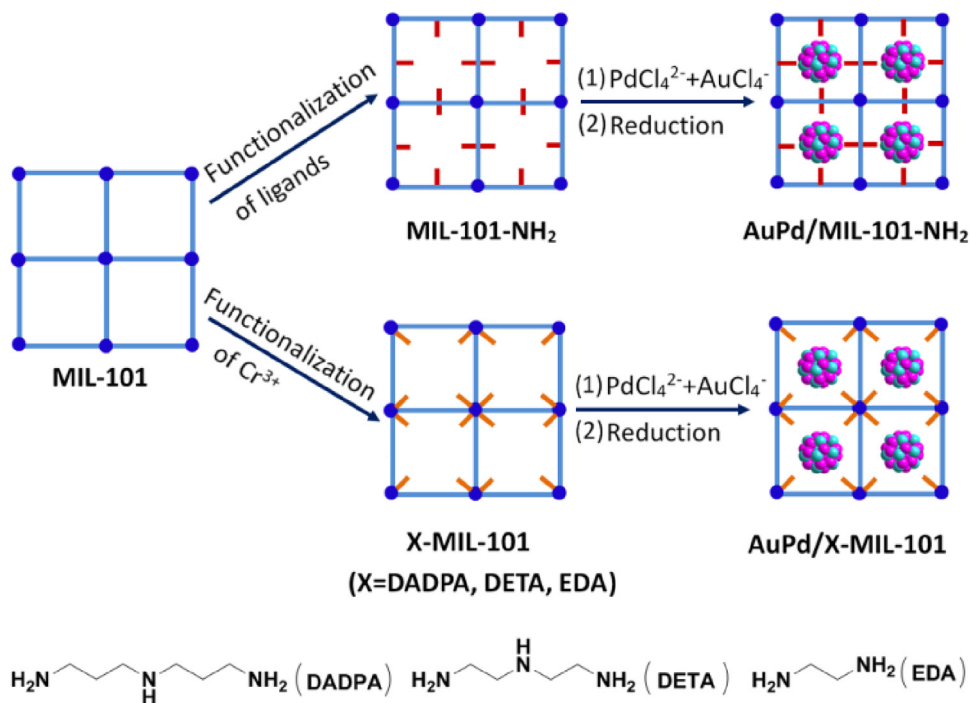


**Fig. 1.** Schematic illustration of modifying the organic linkers and unsaturated metal coordination Cr<sup>3+</sup> sites in MIL-101 and preparing AuPd NPs immobilized by the two types of functional MIL-101 frameworks.

### 2.3. Calculation method

The turnover frequency (TOF) was calculated from the equation as follow:

$$\text{TOF} = \frac{P_{\text{atm}} V_{\text{gas}} / RT}{2n_{\text{metal}} t}$$

In the equation,  $P_{\text{atm}}$  is the atmospheric pressure in Hohhot of Inner Mongolia,  $V_{\text{gas}}$  is the volume of generated H<sub>2</sub> and CO<sub>2</sub>,  $R$  is the universal gas constant (8.314 m<sup>3</sup> Pa mol<sup>-1</sup> K<sup>-1</sup>),  $T$  is the room temperature (298 K),  $n_{\text{metal}}$  is the total molar amounts of noble metals in the catalyst, and  $t$  is the reaction time.

### 2.4. Catalyst characterization

The transmission electron microscopy (TEM, JEM-2010) equipped with an energy dispersive X-ray spectroscopy (EDS) for elemental analysis was applied to check the morphologies and compositions of the samples. Powder X-ray diffraction (PXRD) measurements were performed on a Panalytical X-Pert X-ray diffractometer. The surface area measurements were performed by N<sub>2</sub> adsorption/desorption at liquid N<sub>2</sub> temperature (77 K) after dehydration under vacuum at 150 °C for 12 h using an automatic volumetric adsorption equipment (Autosorb-iQ2-MP). The X-ray photoelectron spectra (XPS) analyses were carried out on an ESCALAB250 (Thermo VG Corp.) equipped with an Al-K $\alpha$  X-ray excitation source. Detailed analyses for CO<sub>2</sub>, H<sub>2</sub> and CO were performed on a Shimadzu gas chromatograph (GC-2014) with thermal conductivity detector (TCD) and hydrogen flame ionization detector (FID)-methanator (detection limit: ~10 ppm). The IR spectra were recorded on an infrared spectrometer (Thermo Fisher Scientific, NEXUS-670) in the wavenumber range of 400–4000 cm<sup>-1</sup>. The UV-vis spectra were conducted on a spectrometer (Shimadzu UV-3600). The nuclear magnetic resonance (NMR) spectra were acquired on a spectrometer (Bruker Advance III 500) and the chemical shifts were reported relative to a residual solvent peak (D<sub>2</sub>O = 4.9 ppm for <sup>1</sup>H).

## 3. Results and discussion

### 3.1. Synthesis

In the heterogeneous catalytic system, the chemical environment surrounding the active metal NPs influences the catalytic performance, such as activity and selectivity. There are two catalytic steps for the decomposition of FA using supported catalysts, the deprotonation of FA to form metal-formate intermediates and the following C–H bond cleavage to release H<sub>2</sub> and CO<sub>2</sub>, which determine the efficiency of FA dehydrogenation [53–63]. To ensuring the above two catalytic steps go well, regulating the chemical environment of active metal NPs would become very important. In fact, once the active species such as AuPd NPs are definitely fixed, the compositions and structures of supports would be the key because the chemical environment of AuPd NPs can only be regulated by their supports. Also, the interaction between the active metal NPs and the supports can be tuned through supports. Herein, we focused on the steric and electronic effects of functional MOFs, which were used to immobilize AuPd NPs for catalytic FA dehydrogenation at 298 K. MIL-101 was selected as catalyst support since it has high porosity, organic terephthalate linkers, unsaturated coordination Cr<sup>3+</sup> sites and high chemical stability [70]. More importantly, the organic linkers and unsaturated coordination Cr<sup>3+</sup> sites in the framework can be modified by electron-donating NH<sub>2</sub> groups or organic amine molecules, respectively [71,72]. Through tuning the steric and electronic effects of MIL-101 frameworks containing different functional groups, the different chemical environment of catalytic active AuPd NPs and the different interaction between AuPd NPs and functional MIL-101 supports could be regulated, resulting in the high-performance H<sub>2</sub> evolution from FA. In general, the high electronic density of active metal NPs is beneficial for the catalytic activity in the catalytic systems, which require the enriched electron environment [73–79]. However, if there is the large steric hindrance around metal NPs, the reaction molecules will difficultly contact with their surface and then the low catalytic activity will be obtained. Therefore, the final catalytic performance

of this type of catalysts is not dependent on the single effect, but the synergistic steric and electronic effects in the catalytic process. By modifying the organic linkers and unsaturated metal coordination  $\text{Cr}^{3+}$  sites in MIL-101 using  $\text{NH}_2$  groups and the different organic amine molecules DADPA, DETA and EDA, respectively, the different chemical environment was created in the AuPd NPs immobilized by these functional MIL-101 supports. On the basis of the functionalization of MIL-101 supports and the resulting synergistic steric and electronic effects, the catalytic performance of supported AuPd NPs on FA dehydrogenation could be tuned. It is known that the reduction half-reaction in  $\text{HCOOH} \rightarrow \text{H}_2 + \text{CO}_2$  dominates the final performance of  $\text{H}_2$  evolution from FA [53–63]. So, the functional MIL-101-supported AuPd NPs with high electron density and low steric hindrance would exhibit high activity in  $\text{H}_2$  evolution from FA. The functionalization of MIL-101 and the synthesis of the supported AuPd catalysts were illustrated in Fig. 1.

### 3.2. Characterization

The  $\text{N}_2$  adsorption/desorption results showed that the surface areas of DADPA-MIL-101, DETA-MIL-101 EDA-MIL-101 and MIL-101-NH<sub>2</sub> decreased compared with bare MIL-101, which revealed the incorporation of functional groups into the MIL-101 frameworks (Fig. S1). This conclusion was further confirmed by both XPS survey patterns and IR spectra, where the N species was checked (Fig. S2) and there were the bending frequency band of N–H at 1588 cm<sup>-1</sup> and the stretching vibration of C–N at 1260 cm<sup>-1</sup> in the functional MIL-101 supports containing NH<sub>2</sub> groups (Fig. S3 and S4). In addition, the PXRD pattern and the  $\text{N}_2$  adsorption/desorption isotherms of MIL-101-NO<sub>2</sub> showed that the framework structure of MIL-101-NO<sub>2</sub> was maintained after the nitration of MIL-101 (Fig. S5 and S6), ensuring the complete formation of MIL-101-NH<sub>2</sub> under the present reduction condition. The functional ratios of organic linkers and unsaturated coordination metal sites were quantified by <sup>1</sup>H NMR upon digestion of the organic species and the corresponding MOFs with KOH in D<sub>2</sub>O (Fig. S7 and S8) [78,79]. The results showed that the percentages of the modified groups or molecules in MIL-101-NH<sub>2</sub>, DADPA-MIL-101, DETA-MIL-101 and EDA-MIL-101 were 100, 90.2, 86.9 and 92, respectively. The XPS results of the Au 4f and Pd 3d of Au<sub>1</sub>Pd<sub>1.5</sub>/MIL-101-NH<sub>2</sub>, Au<sub>1</sub>Pd<sub>1.5</sub>/DADPA-MIL-101, Au<sub>1</sub>Pd<sub>1.5</sub>/EDTA-MIL-101, Au<sub>1</sub>Pd<sub>1.5</sub>/EDA-MIL-101 and Au<sub>1</sub>Pd<sub>1.5</sub>/MIL-101 showed that there were differences in the chemical states of Au and Pd, indicating the different chemical environment of AuPd NPs in these catalysts (Fig. 2). In detail, (i) compared with Au<sub>1</sub>Pd<sub>1.5</sub>/MIL-101, the electron binding energy of Au and Pd in Au<sub>1</sub>Pd<sub>1.5</sub>/MIL-101-NH<sub>2</sub>, Au<sub>1</sub>Pd<sub>1.5</sub>/DADPA-MIL-101, Au<sub>1</sub>Pd<sub>1.5</sub>/EDTA-MIL-101 and Au<sub>1</sub>Pd<sub>1.5</sub>/EDA-MIL-101 decreased due to the presence of the electron-donating NH<sub>2</sub> groups in the functional supports, illustrating that electronic density of Au and Pd was enriched; (ii) Au and Pd species in Au<sub>1</sub>Pd<sub>1.5</sub>/EDA-MIL-101 had the highest electron density due to the strong interaction between AuPd NPs and EDA-MIL-101, which was illustrated in the following section (Fig. 9b).

As shown in Fig. 3 and S9, the AuPd NPs were well dispersed and their sizes in Au<sub>1</sub>Pd<sub>1.5</sub>/MIL-101-NH<sub>2</sub>, Au<sub>1</sub>Pd<sub>1.5</sub>/DADPA-MIL-101, Au<sub>1</sub>Pd<sub>1.5</sub>/DETA-MIL-101, Au<sub>1</sub>Pd<sub>1.5</sub>/EDA-MIL-101 and Au<sub>1</sub>Pd<sub>1.5</sub>/MIL-101 were  $2.2 \pm 0.5$ ,  $2.1 \pm 0.4$ ,  $1.8 \pm 0.4$ ,  $1.5 \pm 0.3$  and  $2.1 \pm 0.4$  nm, respectively. It is known that the structure of MIL-101 has two types of mesoporous cages and their free diameters are ca. 2.9 and 3.4 nm. From the above TEM results, it could be deduced that most of the AuPd NPs were inside the cages of MIL-101 supports in the catalysts. In addition, there were a few AuPd NPs with large size in the catalysts, indicating that these aggregated AuPd NPs were outside the cages of supports. The EDS patterns showed the presence of Au, Pd, Cr, C, N and O in the catalysts (Fig. S10–14). As we know, the microstructures of bimetallic NPs have

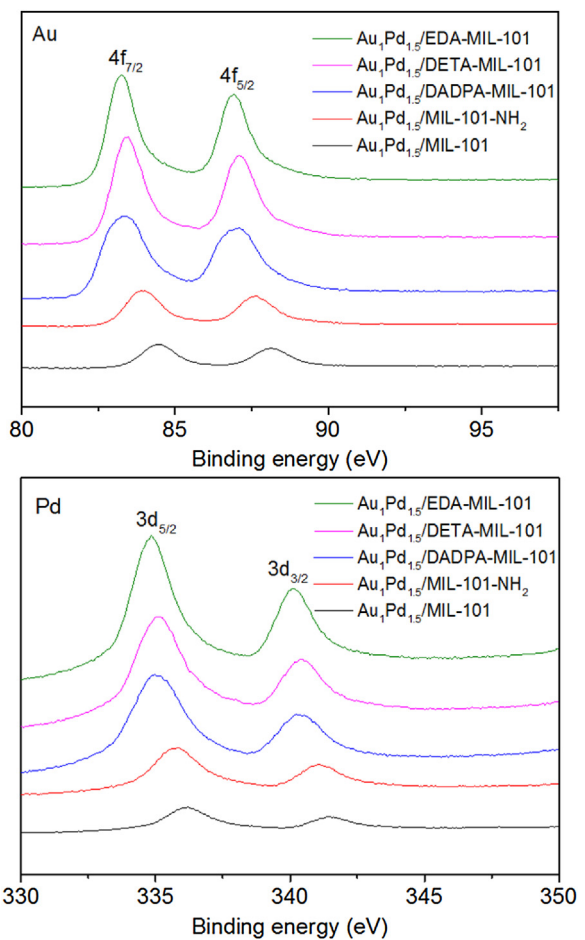


**Fig. 2.** XPS patterns in Au 4f and Pd 3d regions of different catalysts.

significantly affected the catalytic performance. Herein, we investigated the microstructures of AuPd NPs in Au<sub>1</sub>Pd<sub>1.5</sub>/MIL-101-NH<sub>2</sub> and Au<sub>1</sub>Pd<sub>1.5</sub>/MIL-101 using the high-resolution TEM (HRTEM) and the high-angle annular dark-field scanning TEM (HAADF-STEM) (Fig. 4 and S15). The HRTEM image revealed the lattice spacing was measured to be 0.230 nm (Fig. 4a), which was similar to that of the (111) plane of face-centered cubic (fcc) Au (0.235 nm). The elemental maps showed that the metal and non-metal elements were homogeneously distributed in the randomly selected area (Fig. 4c–h and S15b–f). These results indicated the formation of homogeneous AuPd alloy NPs. Moreover, the alloy structures of AuPd NPs were also confirmed by the PXRD results, where a broad peak existed between the characteristic peaks of Au (111) and Pd (111) (Fig. S17). From the ICP results, it was found the noble metal loading amounts were similar to the theoretical values in the catalysts (Table S1).

### 3.3. Catalytic performance

#### 3.3.1. FA dehydrogenation over different catalysts

In order to explore the influence of chemical environment of AuPd NPs on FA dehydrogenation, Au<sub>1</sub>Pd<sub>1.5</sub>/MIL-101-NH<sub>2</sub>, Au<sub>1</sub>Pd<sub>1.5</sub>/DADPA-MIL-101, Au<sub>1</sub>Pd<sub>1.5</sub>/DETA-MIL-101, Au<sub>1</sub>Pd<sub>1.5</sub>/EDA-MIL-101 and Au<sub>1</sub>Pd<sub>1.5</sub>/MIL-101 were used to check the hydrogen evolution performance. The results showed that the five catalysts had remarkably different activities and H<sub>2</sub> selectivities in the decomposition of FA at 298 K (Fig. 5 and S18). Notably, Au<sub>1</sub>Pd<sub>1.5</sub>/MIL-101 had the lowest activity and Au<sub>1</sub>Pd<sub>1.5</sub>/MIL-101-NH<sub>2</sub> had the highest activity featuring initial

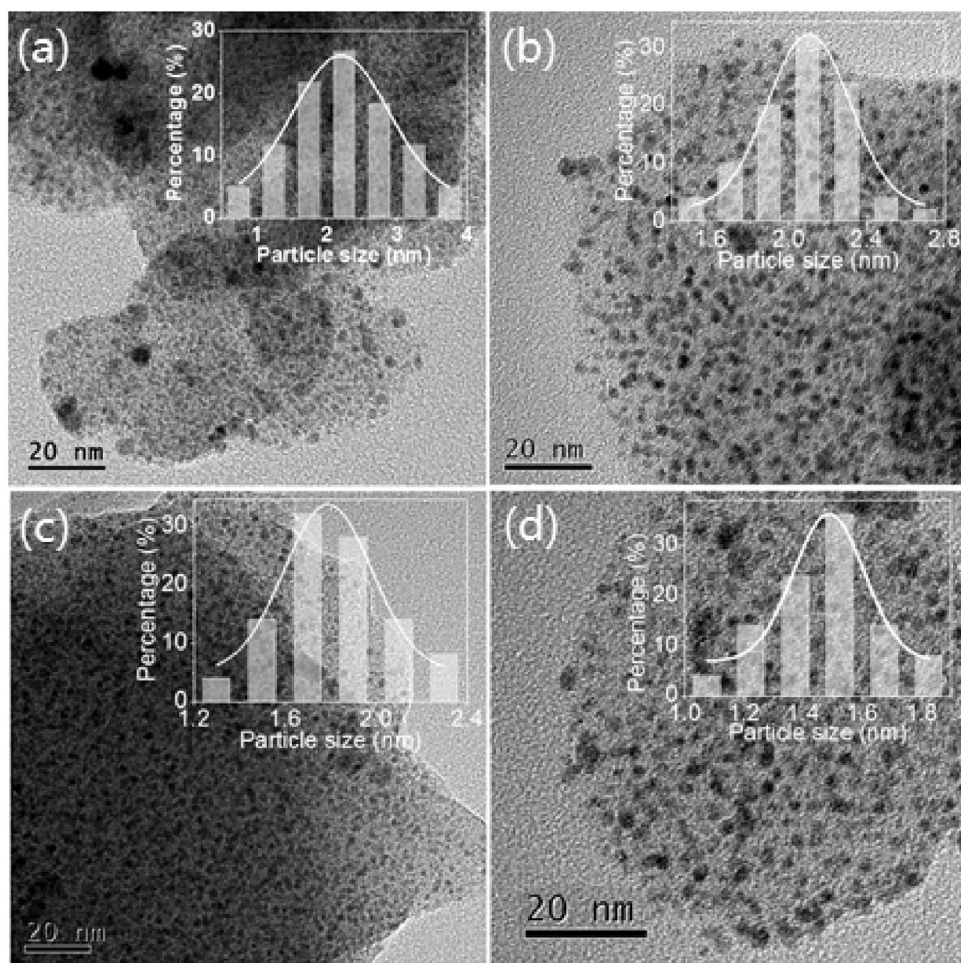


**Fig. 3.** TEM images of (a)  $\text{Au}_{1.5}/\text{MIL}-101-\text{NH}_2$ , (b)  $\text{Au}_{1.5}/\text{DADPA-MIL}-101$ , (c)  $\text{Au}_{1.5}/\text{DETA-MIL}-101$  and (d)  $\text{Au}_{1.5}/\text{EDA-MIL}-101$ . Inset: Corresponding size distributions of AuPd NPs.

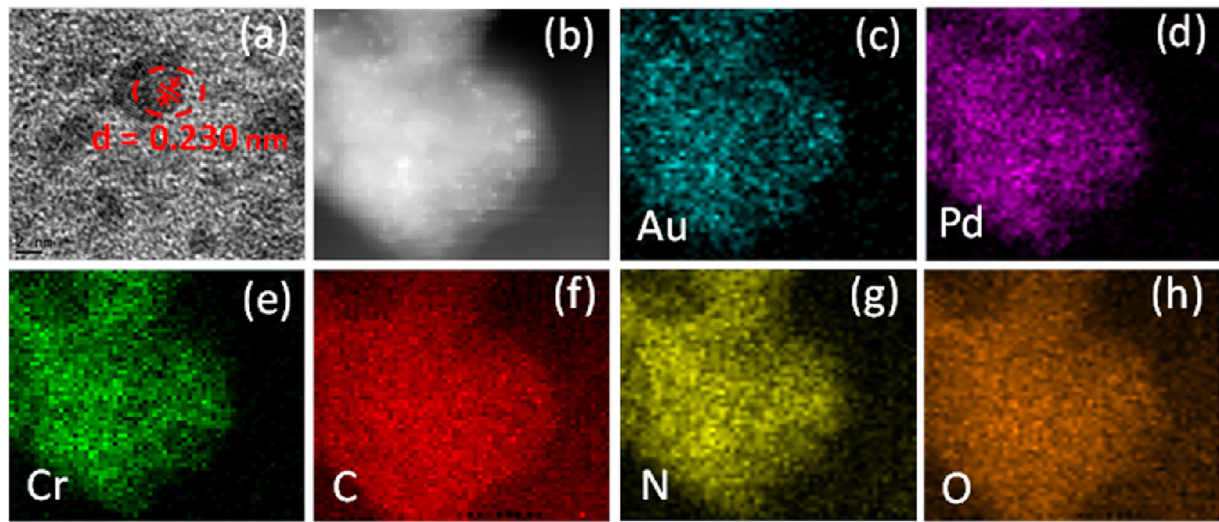


**Fig. 4.** (a) HRTEM and (b) HAADF-STEM images of  $\text{Au}_{1.5}/\text{MIL}-101-\text{NH}_2$  and the corresponding elemental maps for (c) Au, (d) Pd, (e) Cr, (f) C, (g) N and (h) O.

TOF value of  $526 \text{ h}^{-1}$  at 298 K in the five catalysts, which was comparable to the values acquired from the heterogeneous metal catalysts at 298 K [41–63], i.e.,  $\text{Au/ZrO}_2$  ( $252 \text{ h}^{-1}$ ) [45],  $\text{Pd/SBA-15-Amine}$  ( $293 \text{ h}^{-1}$ ) [51],  $\text{Ag}_{0.1}\text{Pd}_{0.9}/\text{RGO}$  ( $453 \text{ h}^{-1}$ ) [59] and  $\text{Au}_{0.75}\text{Pd}_{0.25}/\text{C-L-7.5}$  ( $718 \text{ h}^{-1}$ ) [61] (Table S2). It should be noted

that 445 mL of  $\text{CO}_2$  and  $\text{H}_2$  generated from the decomposition of FA and other 23 mL of  $\text{H}_2$  contributed by the hydrolysis of SF (Fig. S19), indicating the complete and efficient conversion of FA into  $\text{H}_2$  and  $\text{CO}_2$ . Moreover, the activities of three catalysts  $\text{Au}_{1.5}/\text{DADPA-MIL}-101$ ,  $\text{Au}_{1.5}/\text{DETA-MIL}-101$  and  $\text{Au}_{1.5}/\text{EDA-MIL}-101$

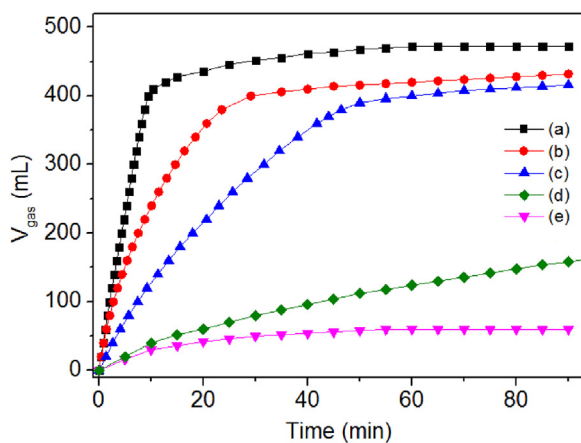


**Fig. 5.** Plots of time versus volume of the generated gas ( $\text{H}_2$  and  $\text{CO}_2$ ) from FA-SF aqueous solution over (a)  $\text{Au}_1\text{Pd}_{1.5}/\text{MIL}-101-\text{NH}_2$ , (b)  $\text{Au}_1\text{Pd}_{1.5}/\text{DADPA}-\text{MIL}-101$ , (c)  $\text{Au}_1\text{Pd}_{1.5}/\text{DETA}-\text{MIL}-101$ , (d)  $\text{Au}_1\text{Pd}_{1.5}/\text{EDA}-\text{MIL}-101$  and (e)  $\text{Au}_1\text{Pd}_{1.5}/\text{MIL}-101$  at 298 K.

fell in between  $\text{Au}_1\text{Pd}_{1.5}/\text{MIL}-101-\text{NH}_2$  and  $\text{Au}_1\text{Pd}_{1.5}/\text{MIL}-101$  and they also had the remarkably different activities. Besides these different activities, the  $\text{H}_2$  selectivities of the five catalysts were also different. The  $\text{H}_2$  selectivities of  $\text{Au}_1\text{Pd}_{1.5}/\text{DADPA}-\text{MIL}-101$ ,  $\text{Au}_1\text{Pd}_{1.5}/\text{DETA}-\text{MIL}-101$ ,  $\text{Au}_1\text{Pd}_{1.5}/\text{EDA}-\text{MIL}-101$  and  $\text{Au}_1\text{Pd}_{1.5}/\text{MIL}-101$  were 94, 89, 85 and 13%, respectively, which were lower than the value (100%) of  $\text{Au}_1\text{Pd}_{1.5}/\text{MIL}-101-\text{NH}_2$ . The catalytic performance of the five monometallic Pd catalysts containing different functional groups ( $\text{Pd}/\text{MIL}-101-\text{NH}_2$ ,  $\text{Pd}/\text{DADPA}-\text{MIL}-101$ ,  $\text{Pd}/\text{DETA}-\text{MIL}-101$ ,  $\text{Pd}/\text{EDA}-\text{MIL}-101$  and  $\text{Pd}/\text{MIL}-101$ ) was also tested. The results showed that the catalytic activity orderliness of the five monometallic Pd catalysts was similar to that of the five bimetallic AuPd catalysts (Fig. S20). All the different catalytic performance (activity and selectivity) indicated that the whole chemical environment of metal NPs immobilized by different supports was different. The above activity orderliness of different catalysts could be explained by the absence or presence of  $\text{NH}_2$  groups in MIL-101 frameworks as well as the steric and electronic effects of functional MIL-101 frameworks. Regarding the effect of  $\text{NH}_2$  groups in MIL-101 on FA dehydrogenation, it was found that  $\text{NH}_2$  groups could enhance the catalytic activity. This phenomenon can also be found in the heterogeneous catalysis using supported metal catalysts containing inorganic supports such as  $\text{SiO}_2$  functionalized by  $\text{NH}_2$  [80–83]. The steric and electronic effects of functional MIL-101 on FA dehydrogenation were elaborated below (Fig. 9b). In many cases, the small size of active metal NPs always favors the high catalytic performance [53–63]. Herein, although the size of AuPd NPs in

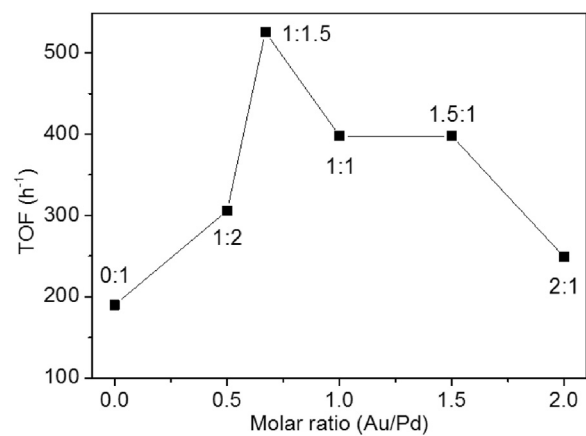


**Fig. 7.** Initial TOF values of  $\text{Au}_x\text{Pd}_y/\text{MIL}-101-\text{NH}_2$  with different molar ratios of Au/Pd at 298 K.

$\text{Au}_1\text{Pd}_{1.5}/\text{MIL}-101-\text{NH}_2$  was bigger than that in the AuPd catalysts based on other three functional supports (Fig. 3), the activity of  $\text{Au}_1\text{Pd}_{1.5}/\text{MIL}-101-\text{NH}_2$  was the highest among all the catalysts, indicating that the functionalization of MIL-101 in the catalysts was the key to determining the catalytic performance, but not the size of AuPd NPs.

The GC analysis showed that there was no CO detected in the mixture of  $\text{H}_2$  and  $\text{CO}_2$  (Fig. 6a), which was crucial for fuel cell applications [41–63]. Moreover, the GC analysis confirmed that the molar ratios of  $\text{H}_2/\text{CO}_2$  in the gas mixture generated from FA-SF solution catalyzed by  $\text{Au}_1\text{Pd}_{1.5}/\text{MIL}-101-\text{NH}_2$  and  $\text{Au}_1\text{Pd}_{1.5}/\text{DADPA}-\text{MIL}-101$  were about 1.11 and 1.06, respectively (Fig. 6b). This indicated that the dehydrogenation pathway happened in the reaction of FA decomposition though the  $\text{H}_2$  selectivity of  $\text{Au}_1\text{Pd}_{1.5}/\text{DADPA}-\text{MIL}-101$  was 94% and 11 mL of  $\text{H}_2$  contributed by the hydrolysis of SF (Fig. S21).

Besides the positions and structures of functional groups in the isoreticular MOFs, other factors such as the electronic characteristics of functional groups and the framework structures of MOFs also significantly affected the catalytic performance of corresponding catalysts [25–32]. To investigate the electronic effect of functional groups on catalysis, the organic linker in MIL-101 was modified by electro-accepting  $\text{NO}_2$  to obtain MIL-101- $\text{NO}_2$ , which was used as support to synthesize AuPd catalyst. The TEM investigation showed that the average size of AuPd NPs in  $\text{Au}_1\text{Pd}_{1.5}/\text{MIL}-101-\text{NO}_2$  was  $3.1 \pm 0.3$  nm (Fig. S22), which was slightly bigger than that in  $\text{Au}_1\text{Pd}_{1.5}/\text{MIL}-101-\text{NH}_2$ . However, the catalytic results showed that  $\text{Au}_1\text{Pd}_{1.5}/\text{MIL}-101-\text{NO}_2$  had drastically lower activity and  $\text{H}_2$  selectivity than  $\text{Au}_1\text{Pd}_{1.5}/\text{MIL}-101-\text{NH}_2$  (Fig. S24). From this comparison, it could be clearly found that the presence of electron-donating

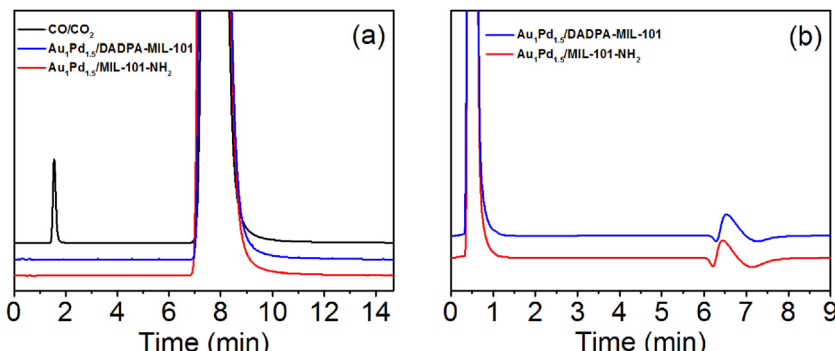


**Fig. 6.** GC spectra obtained using (a) FID-methanator for the mixture of CO and  $\text{CO}_2$  with 100 ppm of CO and the evolved gas and (b) TCD for the evolved gas from FA-SF aqueous solution over two types of catalysts at 298 K.

$\text{NH}_2$  groups in the catalyst support was crucial for enhanced dehydrogenation of FA. In order to further confirm this conclusion, we chose bare MOF-5 and  $\text{NH}_2$ -functionalized MOF-5 (MOF-5- $\text{NH}_2$ ) as supports to prepare AuPd catalysts. The catalytic results showed that  $\text{Au}_{1.5}\text{Pd}_{1.5}/\text{MOF-5-NH}_2$  had much higher activity than  $\text{Au}_{1.5}\text{Pd}_{1.5}/\text{MOF-5}$  (Fig. S25). In order to check whether the  $\text{NH}_2$  groups in the inorganic supports were also crucial for FA dehydrogenation, we selected  $\text{SiO}_2$  (SBA-15) and  $\text{NH}_2$ -functionalized SBA-15 (SBA-15- $\text{NH}_2$ ) as supports to synthesize AuPd catalysts and examined their catalytic properties. The results showed that  $\text{Au}_{1.5}\text{Pd}_{1.5}/\text{SBA-15}$  almost had no activity and  $\text{Au}_{1.5}\text{Pd}_{1.5}/\text{SBA-15-NH}_2$  had relatively high activity and 85% of  $\text{H}_2$  selectivity (Fig. S30). The above results confirmed that the electron-donating  $\text{NH}_2$  groups in all the supports indeed drastically enhanced the performance in the decomposition of FA into  $\text{H}_2$  and MIL-101- $\text{NH}_2$  was the optimal support for immobilizing active metal NPs.

### 3.3.2. Influence of the molar ratios of Au/Pd

The catalytic performance was optimized by tuning the molar ratios of Au/Pd in AuPd NPs immobilized by MIL-101- $\text{NH}_2$ . The results showed that the activity increased with decreasing the content of Pd, when the molar ratio of Au/Pd increased to 1:1.5, the highest catalytic activity reached, but continuing to increase the molar ratio of Au/Pd resulted in the decrease of the activity (Fig. 7 and S35). However, the  $\text{H}_2$  selectivities of all the catalysts with different molar ratios of Au/Pd were kept at 100%. These phenomena indicated that the interaction among different metals also played an important role in the enhanced catalytic performance of heterometallic nanocatalysts.

### 3.3.3. Influence of reaction temperatures

The reaction temperature greatly affected the  $\text{H}_2$  evolution rates [41–63]. The catalytic dehydrogenation rates of FA over AuPd/MIL-101- $\text{NH}_2$  at different temperatures were investigated (Fig. 8a). The results showed that the  $\text{H}_2$  evolution rate increased when the temperature increased from 298 to 323 K, indicating that the high reaction temperature was beneficial for enhancing the dehydrogenation rate of FA. According to the Arrhenius plot, the reaction rate had a near linear dependency on the reaction temperature. The obtained apparent activation energy ( $E_a$ ) of AuPd/MIL-101- $\text{NH}_2$  was calculated to be  $32.5 \text{ kJ mol}^{-1}$ , lower than most of the reported values, indicating that the highly efficient  $\text{H}_2$  evolution from FA could be easily obtained at convenient temperature and the higher reaction temperature could lead to the higher activity of catalyst (Fig. 8b).

### 3.3.4. Recycle stability

The recycle stability is of crucial importance on the practical application of catalysts, so the durability test of FA dehydrogenation over AuPd/MIL-101- $\text{NH}_2$  was carried out at 298 K by adding the same amount of FA into the reactor after the completion of the first run. No significant change of the activity and  $\text{H}_2$  selectivity was found (Fig. S36). Meanwhile, the TEM results showed that after the catalytic reaction, the size distribution of AuPd NPs in AuPd/MIL-101- $\text{NH}_2$  and the morphology of the catalysts remained unchanged, suggesting that the AuPd NPs immobilized by MIL-101- $\text{NH}_2$  possessed high stability during FA decomposition (Fig. S37).  $\text{Au}_{1.5}\text{Pd}_{1.5}/\text{MIL-101-NH}_2$  and  $\text{Au}_{1.5}\text{Pd}_{1.5}/\text{DADPA-MIL-101}$  were selected as examples to check the long-time durability of catalysts. The catalytic results showed that the activities of  $\text{Au}_{1.5}\text{Pd}_{1.5}/\text{MIL-101-NH}_2$  and  $\text{Au}_{1.5}\text{Pd}_{1.5}/\text{DADPA-MIL-101}$  decreased after ten and six cycles (1380 and 950 min), respectively, and  $\text{Au}_{1.5}\text{Pd}_{1.5}/\text{MIL-101-NH}_2$  had the higher long-time durability than  $\text{Au}_{1.5}\text{Pd}_{1.5}/\text{DADPA-MIL-101}$  (Fig. S39). The PXRD results showed that the crystallinity of MIL-101- $\text{NH}_2$  and DADPA-MIL-101 in the catalysts decreased after several catalytic cycles, which was probably

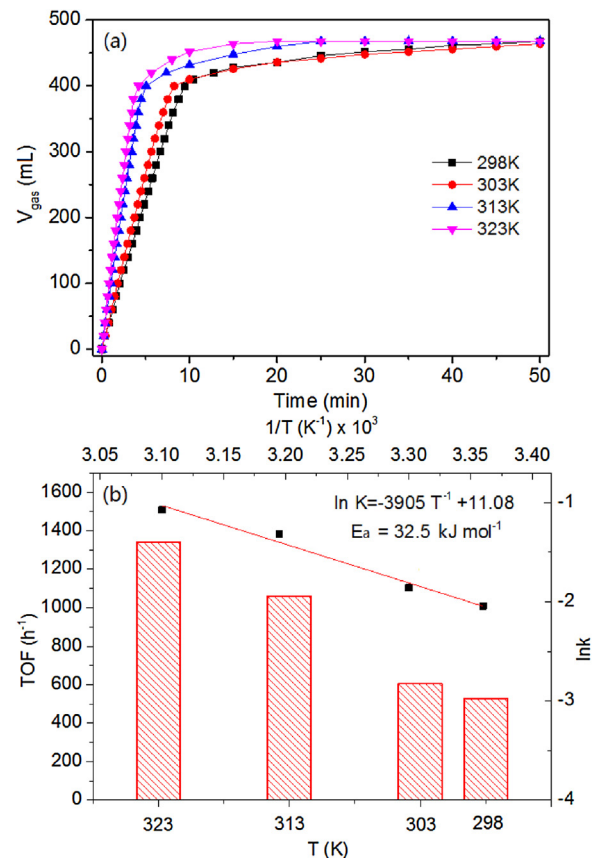


**Fig. 8.** (a) Plots of time versus volume of the generated gas ( $\text{H}_2$  and  $\text{CO}_2$ ) from FA aqueous solution over  $\text{Au}_{1.5}\text{Pd}_{1.5}/\text{MIL-101-NH}_2$  at different temperatures and (b) Arrhenius plot and TOF values of  $\text{Au}_{1.5}\text{Pd}_{1.5}/\text{MIL-101-NH}_2$ .

due to that the acidic catalytic substrate partly destroyed the porosity of MIL-101 (Fig. S40). The  $\text{N}_2$  adsorption/desorption results of both catalysts also testified these results (Fig. S41). In addition, there were some serious aggregations of AuPd NPs in the spent catalysts after several catalytic cycles (Fig. S42), which also influenced and decreased the activities of catalysts.

### 3.4. Catalytic mechanism

For the FA decomposition, the activities and  $\text{H}_2$  selectivities of catalysts were strongly related with the activation of FA molecule [41–63], which depends on the steric and electronic environment of active metal NPs. As illustrated in Fig. 9a, firstly, due to the presence of  $\text{NH}_2$  groups on the catalyst surface, the electronegative N atoms in  $\text{NH}_2$  groups in MIL-101, as proton scavengers, facilitated the O–H bond cleavage in the FA molecule, leading to the formation of intermediates  $\text{AuPd}-\text{OOCH}^-$  and  $[\text{H}_2\text{NH}]^+$ . Secondly, the hydride elimination happened in the  $\text{AuPd}-\text{OOCH}^-$  species to produce  $\text{CO}_2$  and  $\text{AuPd}-\text{H}^-$  species. Finally,  $\text{H}_2$  produced through the hydrogen desorption of  $[\text{H}_2\text{NH}]^+$  and  $\text{AuPd}-\text{H}^-$  species. This mechanism was supported by the above catalytic results that  $\text{AuPd}/\text{MIL-101}$  without  $\text{NH}_2$  groups had very low activity and  $\text{H}_2$  selectivity, but AuPd NPs supported by MIL-101- $\text{NH}_2$  had high activity and 100% of  $\text{H}_2$  selectivity. For the synergistic steric and electronic effects of functional MIL-101 frameworks on FA dehydrogenation, it could be explained as following. Since the organic linker 1,4-dicarboxybenzoate has higher electron density than inorganic ion  $\text{Cr}^{3+}$  in the MIL-101 framework, the electronic density of the  $\text{NH}_2$  groups in MIL-101- $\text{NH}_2$  would be theoretically higher than that in DADPA-101- $\text{NH}_2$ , DETA-101- $\text{NH}_2$  and EDA-

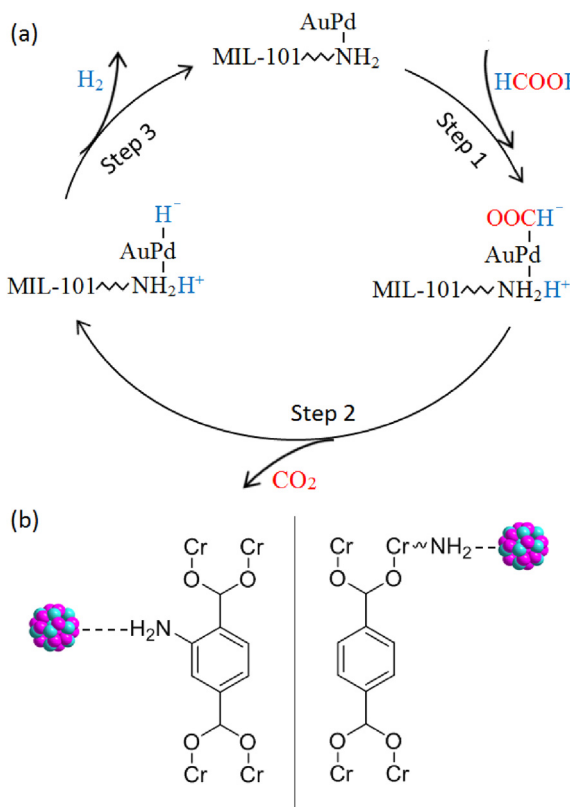


**Fig. 9.** (a) Possible activation pathways of the FA molecule in the reaction using the catalysts containing functional groups and (b) the schematic illustration for the interaction modes between AuPd NPs and functional MIL-101 frameworks in the catalysts.

101-NH<sub>2</sub>. However, the coordination between metal species and NH<sub>2</sub> groups in MIL-101-NH<sub>2</sub> was much more difficult than that between metal ions and another type of functional MIL-101 frame-

works (DADPA, DETA or EDA) due to the large steric hindrance. Based on this fact, it could be induced that AuPd NPs and the NH<sub>2</sub> groups in Au<sub>1</sub>Pd<sub>1.5</sub>/MIL-101-NH<sub>2</sub> could not effectively contact (Fig. 9b), resulting in that the electron density of Au and Pd species in Au<sub>1</sub>Pd<sub>1.5</sub>/MIL-101-NH<sub>2</sub> was lower than that in Au<sub>1</sub>Pd<sub>1.5</sub>/DADPA-MIL-101, Au<sub>1</sub>Pd<sub>1.5</sub>/DETA-MIL-101 and Au<sub>1</sub>Pd<sub>1.5</sub>/EDA-MIL-101, but was still higher than that in NH<sub>2</sub>-free Au<sub>1</sub>Pd<sub>1.5</sub>/MIL-101. This orderliness was verified by the XPS results (Fig. 2). However, just because MIL-101-NH<sub>2</sub> had much relatively weak interaction with AuPd NPs in comparison with DADPA-MIL-101, DETA-MIL-101 and EDA-MIL-101, small molecule FA with acidity was easily accessible to contact the NH<sub>2</sub> groups in Au<sub>1</sub>Pd<sub>1.5</sub>/MIL-101-NH<sub>2</sub>, resulting in the stronger ability of Au<sub>1</sub>Pd<sub>1.5</sub>/MIL-101-NH<sub>2</sub> to activate FA than that of Au<sub>1</sub>Pd<sub>1.5</sub>/DADPA-MIL-101, Au<sub>1</sub>Pd<sub>1.5</sub>/DETA-MIL-101 and Au<sub>1</sub>Pd<sub>1.5</sub>/EDA-MIL-101. It is known that the activation of substrate molecules in the heterogeneous catalysis always plays an important role in enhancing the catalytic performance [84–88]. Therefore, in the present catalytic system, the synergistic steric and electron effects of MIL-101 frameworks containing different functional groups led to the different catalytic activities and H<sub>2</sub> selectivities of catalysts, where Au<sub>1</sub>Pd<sub>1.5</sub>/MIL-101-NH<sub>2</sub> had the relatively high electron density and low steric hindrance of AuPd NPs and the resultant highest H<sub>2</sub> evolution activity and selectivity. Moreover, in comparison with DETA and EDA, DADPA featured the non-coordinating NH<sub>2</sub> groups with low steric hindrance for contacting FA molecules and thus had the strong ability to activate FA, leading to the highest activity of Au<sub>1</sub>Pd<sub>1.5</sub>/DADPA-MIL-101 in the three catalysts Au<sub>1</sub>Pd<sub>1.5</sub>/DADPA-MIL-101, Au<sub>1</sub>Pd<sub>1.5</sub>/DETA-MIL-101 and Au<sub>1</sub>Pd<sub>1.5</sub>/EDA-MIL-101. From the above results, we could find that on the premise of the presence of electron-donating NH<sub>2</sub> groups in the catalysts, the steric effect involving the activation of small molecule FA played a key role in the enhanced catalytic performance. Thus, the activation of FA (step 1) could be the rate-determining step in the catalytic pathway of the present supported AuPd catalysts (Fig. 9a). From these analyses, it could be found that the different chemical environment and interaction of AuPd NPs immobilized by the different functional MIL-101 frameworks played an important role for the high H<sub>2</sub> production activity, which

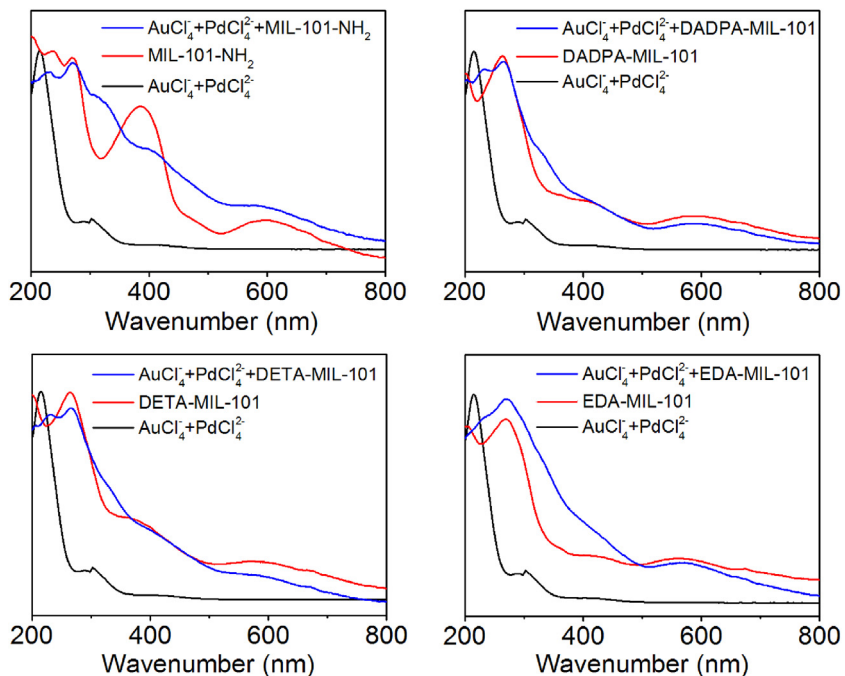


**Fig. 10.** UV-vis spectra of the coordination complexes assembled by various functional MIL-101 frameworks and mixed metal ions (AuCl<sub>4</sub><sup>-</sup> and PdCl<sub>4</sub><sup>2-</sup>).

was verified by the above different catalytic results and the highest activity of AuPd/MIL-101-NH<sub>2</sub>.

In order to figure out the role of different supports in the catalyst formation, we checked the changes of the coordination complex intermediates after the reaction between different functional supports (MIL-101-NH<sub>2</sub>, DADPA-MIL-101, DETA-MIL-101, EDA-MIL-101) and the mixed metal ions (AuCl<sub>4</sub><sup>-</sup> and PdCl<sub>4</sub><sup>2-</sup>) using UV-vis spectroscopy. From the spectra of the coordination complexes, it was found that new characteristic peaks at different wavelengths appeared in every coordination complex (Fig. 10), which could be attributed to the formation of coordination complexes with different structures due to the different interactions between the functional supports and mixed metal ions. So the four different coordination complexes acted as precursors in the subsequent NaBH<sub>4</sub> reduction and induced the formation of AuPd NPs with different chemical environment, which resulted in the different catalytic performance at 298 K.

#### 4. Conclusions

In summary, two different types of porous amine-functionalized MIL-101 supports were selected to synthesize a series of supported bimetallic catalysts, where AuPd NPs immobilized by MIL-101 functionalized by electron-donating NH<sub>2</sub> groups in the organic linkers exhibited 100% of H<sub>2</sub> selectivity and drastically high activity at 298 K. The remarkably different activities and H<sub>2</sub> selectivities of catalysts could be due to the different chemical environment of AuPd NPs immobilized by the different functional MIL-101 frameworks, which resulted in the different activation ability for FA molecules in the catalytic process. In addition, the different interaction between the four different functional MIL-101 supports and mixed metal ions induced the formation of different coordination complex intermediates, which also played an important role in yielding AuPd NPs featuring different chemical environment. Our research provided an understanding of how the functional groups of catalyst supports influence the catalytic activity and H<sub>2</sub> selectivity in FA dehydrogenation in the atomic level at 298 K, thus opening up fascinating opportunities for the development of high-performance and tunable metal/MOFs in various catalytic fields including sustainable energy production and chemical synthesis.

#### Acknowledgements

The authors gratefully acknowledge the financial support from the Program for New Century Excellent Talents in University of the Ministry of Education of China (grant no. NCET-13-0846) and the Program for Young Talents of Science and Technology in Universities of Inner Mongolia Autonomous Region (grant no. NJYT-13-A01).

#### Appendix A. Supplementary data

Supplementary data associated with this article can be found, in the online version, at <http://dx.doi.org/10.1016/j.apcatb.2017.06.084>.

#### References

- [1] R. Subbaraman, D. Tripkovic, K.-C. Chang, D. Strmcnik, A.P. Paulikas, P. Hirunsit, M. Chan, J. Greeley, V. Stamenkovic, N.M. Markovic, *Material* 11 (2012) 550–557.
- [2] C.A. Schoenbaum, D.K. Schwartz, J. Will Medlin, *Acc. Chem. Res.* 47 (2014) 1438–1445.
- [3] Y. Cong, M. Chen, T. Xu, Y. Zhang, Q. Wang, *Appl. Catal. B: Environ.* 147 (2014) 733–740.
- [4] P. Liu, Y. Zhao, R. Qin, S. Mo, G. Chen, L. Gu, D.M. Chevrier, P. Zhang, Q. Guo, D. Zang, B. Wu, G. Fu, N. Zheng, *Science* 352 (2016) 797–801.
- [5] J. Shen, R. Steinbach, J.M. Tobin, M.M. Nakata, M. Bower, M.R.S. McCoustra, H. Bridle, V. Arrighi, F. Vilela, *Appl. Catal. B: Environ.* 193 (2016) 226–233.
- [6] Z. Yang, X. Xu, X. Liang, C. Lei, Y. Wei, P. He, B. Lv, H. Ma, Z. Lei, *Appl. Catal. B: Environ.* 198 (2016) 112–123.
- [7] N. Barhoumi, H. Olvera-Vargas, N. Oturan, D. Huguenot, A. Gadri, S. Ammar, E. Brillas, M.A. Oturan, *Appl. Catal. B: Environ.* 209 (2017) 637–647.
- [8] M.E. Davis, *Nature* 417 (2002) 813–821.
- [9] G. Prieto, J. Zečević, H. Friedrich, K.P. de Jong, P.E. de Jongh, *Nat. Mater.* 12 (2013) 34–39.
- [10] A. Okrut, R.C. Runnebaum, X. Ouyang, J. Lu, C. Aydin, S.-J. Hwang, S. Zhang, O.A. Olatunji-Ojo, K.A. Durkin, D.A. Dixon, B.C. Gates, A. Katz, *Nat. Nanotechnol.* 9 (2014) 459–465.
- [11] L.-Y. Lin, H. Bai, *Appl. Catal. B: Environ.* 148 (2014) 366–376.
- [12] Y. Karatas, A. Bulut, M. Yurderi, I.E. Ertas, O. Alal, M. Gulcan, M. Celebi, H. Kivrak, M. Kaya, M. Zahmakiran, *Appl. Catal. B: Environ.* 180 (2016) 586–595.
- [13] Z. Jane Wang, K.N. Clary, R.G. Bergman, K.N. Raymond, F. Dean Toste, *Nat. Chem.* 5 (2013) 100–103.
- [14] R.C. Rodrigues, C. Ortiz, A. Berenguer-Murcia, R. Torres, R. Fernández-Lafuente, *Chem. Soc. Rev.* 42 (2013) 6290–6307.
- [15] E.B. Corcoran, M.T. Pirnot, S. Lin, S.D. Dreher, D.A. DiRocco, I.W. Davies, S.L. Buchwald, D.W.C. MacMillan, *Science* 353 (2016) 279–283.
- [16] G. Férey, C. Mellot-Draznieks, C. Serre, F. Millange, J. Dutour, S. Surblé, I. Margiolaki, *Science* 309 (2005) 2040–2041.
- [17] Z. Wang, S.M. Cohen, *Chem. Soc. Rev.* 38 (2009) 1315–1329.
- [18] M. O'Keeffe, O.M. Yaghi, *Chem. Rev.* 112 (2012) 675–702.
- [19] A. Schneemann, V. Bon, I. Schwedler, I. Senkovska, S. Kaskel, R.A. Fischer, *Chem. Soc. Rev.* 43 (2014) 6062–6096.
- [20] M. Eddaoudi, D.F. Sava, J.F. Eubank, K. Adil, V. Guillerm, *Chem. Soc. Rev.* 44 (2015) 228–249.
- [21] Y. Gao, S. Li, Y. Li, L. Yao, H. Zhang, *Appl. Catal. B: Environ.* 202 (2017) 165–174.
- [22] C. Racles, M.-F. Zaltariov, M. Iacob, M. Silion, M. Avadanei, A. Bargan, *Appl. Catal. B: Environ.* 205 (2017) 78–92.
- [23] X. Li, Z. Guo, C. Xiao, T.W. Goh, D. Tesfagaber, W. Huang, *ACS Catal.* 4 (2014) 3490–3497.
- [24] Z. Guo, C. Xiao, R.V. Maligal-Ganesh, L. Zhou, T.W. Goh, X. Li, D. Tesfagaber, A. Thiel, W. Huang, *ACS Catal.* 4 (2014) 1340–1348.
- [25] S. Kitagawa, R. Kitaura, S.i. Noro, *Angew. Chem. Int. Ed.* 43 (2004) 2334–2375.
- [26] L.E. Kreto, K. Leong, O.K. Farha, M. Allendorf, R.P. Van Duyne, J.T. Hupp, *Chem. Rev.* 112 (2012) 1105–1125.
- [27] H.R. Moon, D.-W. Lim, M.P. Suh, *Chem. Soc. Rev.* 42 (2013) 1807–1824.
- [28] N.C. Burch, H. Jasuja, K.S. Walton, *Chem. Rev.* 114 (2014) 10575–10612.
- [29] A. Cadiou, K. Adil, P.M. Bhatt, Y. Belmabkhout, M. Eddaoudi, *Science* 353 (2016) 137–140.
- [30] Y. Su, Z. Zhang, H. Liu, Y. Wang, *Appl. Catal. B: Environ.* 200 (2017) 448–457.
- [31] K.M. Choi, K. Na, G.A. Somorjai, O.M. Yaghi, *J. Am. Chem. Soc.* 137 (2015) 7810–7816.
- [32] X. Li, T.W. Goh, L. Li, C. Xiao, Z. Guo, X.C. Zeng, W. Huang, *ACS Catal.* 6 (2016) 3461–3468.
- [33] J. Graetz, *Chem. Soc. Rev.* 38 (2009) 73–82.
- [34] C.W. Hamilton, R.T. Baker, A. Staubiz, I. Manners, *Chem. Soc. Rev.* 38 (2009) 279–293.
- [35] Q. Yao, W. Shi, G. Feng, Z.-H. Lu, X. Zhang, D. Tao, D. Kong, X. Chen, *J. Power Sources* 257 (2014) 293–299.
- [36] M. Yurderi, A. Bulut, I.E. Ertas, M. Zahmakiran, M. Kaya, *Appl. Catal. B: Environ.* 165 (2015) 169–175.
- [37] J. Ding, L. Zhang, Q. Liu, W.-L. Dai, G. Guan, *Appl. Catal. B: Environ.* 203 (2017) 335–342.
- [38] Q.-L. Zhu, Q. Xu, *Energy Environ. Sci.* 8 (2015) 478–512.
- [39] Z. Yue, A. Liu, C. Zhang, J. Huang, M. Zhu, Y. Du, P. Yang, *Appl. Catal. B: Environ.* 201 (2017) 202–210.
- [40] Z. He, J. Fu, B. Cheng, J. Yu, S. Cao, *Appl. Catal. B: Environ.* 205 (2017) 104–111.
- [41] C. Fellay, P.J. Dyson, G. Laurenczy, *Angew. Chem. Int. Ed.* 47 (2008) 3966–3968.
- [42] M. Ojeda, E. Iglesias, *Angew. Chem. Int. Ed.* 48 (2009) 4800–4803.
- [43] A. Boddien, D. Mellmann, F. Gärtner, R. Jackstell, H. Junge, P.J. Dyson, G. Laurenczy, R. Ludwig, M. Beller, *Science* 333 (2011) 1733–1736.
- [44] K. Tedesco, T. Li, S. Jones, C.W.A. Chan, K.M.K. Yu, P.A.J. Bagot, E.A. Marquis, G.D.W. Smith, S.C.E. Tsang, *Nat. Nanotechnol.* 6 (2011) 302–307.
- [45] Q.-Y. Bi, X.-L. Du, Y.-M. Liu, Y. Cao, H.-Y. He, K.-N. Fan, *J. Am. Chem. Soc.* 134 (2012) 8926–8933.
- [46] G. Qin, Y. Zhang, X. Ke, X. Tong, Z. Sun, M. Liang, S. Xue, *Appl. Catal. B: Environ.* 129 (2013) 599–605.
- [47] K. Mori, M. Dojo, H. Yamashita, *ACS Catal.* 3 (2013) 1114–1119.
- [48] P. Richardson, M. Perdigoto, W. Wang, R. Lopes, *Appl. Catal. B: Environ.* 132 (2013) 408–415.
- [49] H. Dai, N. Cao, L. Yang, J. Sun, W. Luo, G. Cheng, *J. Mater. Chem. A* 2 (2014) 11060–11064.
- [50] D. Won, C. Choi, J. Chung, S. Woo, *Appl. Catal. B: Environ.* 158 (2014) 217–223.
- [51] K. Koh, J.-E. Seo, J.H. Lee, A. Goswami, C.W. Yoo, T. Asefa, *J. Mater. Chem. A* 2 (2014) 20444–20449.
- [52] Z. Zhang, S.-W. Cao, Y. Liao, C. Xue, *Appl. Catal. B: Environ.* 162 (2015) 204–209.
- [53] Y. Huang, X. Zhou, M. Yin, C. Liu, W. Xing, *Chem. Mater.* 22 (2010) 5122–5128.
- [54] X. Gu, Z.-H. Lu, H.-L. Jiang, T. Akita, Q. Xu, *J. Am. Chem. Soc.* 133 (2011) 11822–11825.
- [55] Z.-L. Wang, J.-M. Yan, Y. Ping, H.-L. Wang, W.-T. Zheng, Q. Jiang, *Angew. Chem. Int. Ed.* 52 (2013) 4406–4409.

- [56] K. Jiang, K. Xu, S. Zou, W.-B. Cai, J. Am. Chem. Soc. 136 (2014) 4861–4864.
- [57] A. Bulut, M. Yurderi, Y. Karatas, M. Zahmakiran, H. Kivrak, M. Gulcan, M. Kaya, Appl. Catal. B: Environ. 165 (2015) 324–333.
- [58] J.-M. Yan, Z.-L. Wang, L. Gu, S.-J. Li, H.-L. Wang, W.-T. Zheng, Q. Jiang, Adv. Energy Mater. 5 (2015) 1500107.
- [59] Y. Chen, Q.-L. Zhu, N. Tsomori, Q. Xu, J. Am. Chem. Soc. 137 (2015) 106–109.
- [60] N. Wang, Q. Sun, R. Bai, X. Li, G. Guo, J. Yu, J. Am. Chem. Soc. 138 (2016) 7484–7487.
- [61] J. Cheng, X. Gu, X. Sheng, P. Liu, H. Su, J. Mater. Chem. A 4 (2016) 1887–1894.
- [62] P. Liu, X. Gu, H. Zhang, J. Cheng, J. Song, H. Su, Appl. Catal. B: Environ. 204 (2017) 497–504.
- [63] J. Cheng, X. Gu, P. Liu, T. Wang, H. Su, J. Mater. Chem. A 4 (2016) 16645–16652.
- [64] D.J. Gorin, B.D. Sherry, F. Dean Toste, Chem. Rev. 108 (2008) 3351–3378.
- [65] O.P. Krivoruchko, T.V. Larina, R.A. Shutilov, V.Y. Gavrilov, S.A. Yashnik, V.A. Sazonov, I.Y. Molina, Z.R. Ismagilov, Appl. Catal. B: Environ. 103 (2011) 1–10.
- [66] K.C. Harper, M.S. Sigman, Science 333 (2011) 1875–1878.
- [67] J.M. Medina, J.L. Mackey, N.K. Garg, K.N. Houk, J. Am. Chem. Soc. 136 (2014) 15798–15805.
- [68] R. Gutzler, S. Stepanow, D. Grumelli, M. Lingenfelder, K. Kern, Acc. Chem. Res. 48 (2015) 2132–2139.
- [69] G. Palermo, A. Cavalli, M.L. Klein, M. Alfonso-Prieto, M. Dal Peraro, M. De Vivo, Acc. Chem. Res. 48 (2015) 220–228.
- [70] Y.K. Hwang, D.-Y. Hong, J.-S. Chang, S.H. Jhung, Y.-K. Seo, J. Kim, A. Vimont, M. Daturi, C. Serre, G. Férey, Angew. Chem. Int. Ed. 47 (2008) 4144–4148.
- [71] S.M. Cohen, Chem. Rev. 112 (2012) 970–1000.
- [72] Y. Hu, W.M. Verdegaal, S.-H. Yu, H.-L. Jiang, ChemSusChem 7 (2014) 734–737.
- [73] X. Wang, X. Li, L. Zhang, Y. Yoon, P.K. Weber, H. Wang, J. Guo, H. Dai, Science 324 (2009) 768–771.
- [74] H. Tsunoyama, N. Ichikuni, H. Sakurai, T. Tsukuda, J. Am. Chem. Soc. 131 (2009) 7086–7093.
- [75] S. Jones, J. Qu, K. Tedsee, X.-Q. Gong, S.C.E. Tsang, Angew. Chem. Int. Ed. 51 (2012) 11275–11278.
- [76] S. Sarina, H.-Y. Zhu, Q. Xiao, E. Jaatinen, J. Jia, Y. Huang, Z. Zheng, H. Wu, Angew. Chem. Int. Ed. 53 (2014) 2935–2940.
- [77] G. Chen, C. Xu, X. Huang, J. Ye, L. Gu, G. Li, Z. Tang, B. Wu, H. Yang, Z. Zhao, Z. Zhou, G. Fu, N. Zheng, Nat. Mater. 15 (2016) 564–569.
- [78] X. Li, R.V. Zeeland, R.V. Maligal-Ganesh, Y. Pei, G. Power, L. Stanley, W. Huang, ACS Catal. 6 (2016) 6324–6328.
- [79] X. Li, T.W. Goh, C. Xiao, A.L.D. Stanton, Y. Pei, P.K. Jain, W. Huang, ChemNanoMat 2 (2016) 810–815.
- [80] A. Fihri, M. Bouhrara, U. Patil, D. Cha, Y. Sahi, V. Polshettiwar, ACS Catal. 2 (2012) 1425–1431.
- [81] D. Shen, L. Chen, J. Yang, R. Zhang, Y. Wei, X. Li, W. Li, Z. Sun, H. Zhu, A.M. Abdullah, A. Al-Enizi, A.A. Elzathahry, F. Zhang, D. Zhao, ACS Appl. Mater. Inter. 7 (2015) 17450–17459.
- [82] R. van den Berg, T.E. Parmentier, C.F. Elkjær, C.J. Gommes, J. Sehested, S. Helveg, P.E. de Jongh, K.P. de Jong, ACS Catal. 5 (2015) 4439–4448.
- [83] Y. Ding, W. Sun, W. Yang, Q. Li, Appl. Catal. B: Environ. 203 (2017) 372–380.
- [84] A.M. Ruppert, B.M. Weckhuysen, Handbook of Heterogeneous Catalysis, Wiley-VCH, Weinheim, 2008.
- [85] C. Gouliaras, D. Lee, L. Chan, M.S. Taylor, J. Am. Chem. Soc. 133 (2011) 13926–13929.
- [86] M. Richard, F. Can, D. Duprez, S. Gil, A. Giroir-Fendler, N. Bion, Angew. Chem. Int. Ed. 53 (2014) 11342–11345.
- [87] L. Li, J.-J. Chen, Y.-J. Li, X.-B. Bu, Q. Liu, Y.-L. Zhao, Angew. Chem. Int. Ed. 54 (2015) 12107–12111.
- [88] J.D.A. Pelletier, J.-M. Basset, Acc. Chem. Res. 49 (2016) 664–677.